Hypothesis

The structure of the voltage-sensitive sodium channel

Inferences derived from computer-aided analysis of the *Electrophorus electricus* channel primary structure

R.E. Greenblatt*, Y. Blatt*, and M. Montal*+

Departments of +Biology and **Physics, University of California San Diego, La Jolla, CA 92093, USA*

Received 13 August 1985

A variety of computer-aided analyses was applied to the recently derived amino acid sequence of the *Electrophorus electricus* sodium channel protein in order to extract structural information such as hydrophobicity, periodicity, and secondary structure predictors. We propose a schematic model for the arrangement and folding of the polypeptide chain within the bilayer. The model consists of 4 homologous regions, each containing 8 membrane-spanning (probably α-helical) structures. Several of these structures are amphipathic with a repeat of 3.5 residues, 4 of which (one from each homologous region) are postulated to form a negatively charged channel lining. Gating currents are proposed to arise from voltage-dependent separation of multiple ion pairs buried within the hydrophobic, intramembranous protein interior.

Sodium channel *Secondary structure prediction* *Computer modelling* *Membrane protein* *Amphipathic helix*

1. INTRODUCTION

The voltage-sensitive sodium channel allows the inward sodium current to flow across the neuronal membrane during the depolarizing phase of an action potential [1]. The sodium channel protein has been purified [2–5] and its major component is a glycopeptide with an apparent $M_r \sim 260\,000$ [2–5], with ~30% of its mass accounted for by carbohydrate [2,3,5]. Functional reconstitution of the purified sodium channel protein in lipid membranes [6–11] demonstrated that all the functional elements of the sodium channel are inherent to the purified protein.

A central problem in molecular neurobiology is the understanding of the gating kinetics of voltage-sensitive ion channels in terms of underlying protein structures. Recently, Numa and his collaborators [12] derived the primary structure of the *Electrophorus electricus* sodium channel from cDNA sequences. Here, we propose a schematic model for the arrangement and folding of the polypeptide chain within the bilayer based on a variety of computer-aided analyses [13]. A similar approach has suggested models for the *Torpedo californica* acetylcholine receptor which are useful in the design of experiments (e.g. [14–16]). Others have also postulated models of the sodium channel structure [12,17,18], and we compare explicitly some similarities and differences between them.

2. METHODS

2.1. *Programs*

All programs (except for molecular modelling) were written in the 'C' programming language and run under EUNICE (4.2 BSD UNIX under the

+ To whom correspondence and reprint requests should be addressed

Published by Elsevier Science Publishers B.V. (Biomedical Division)
00145793/85/$3.30

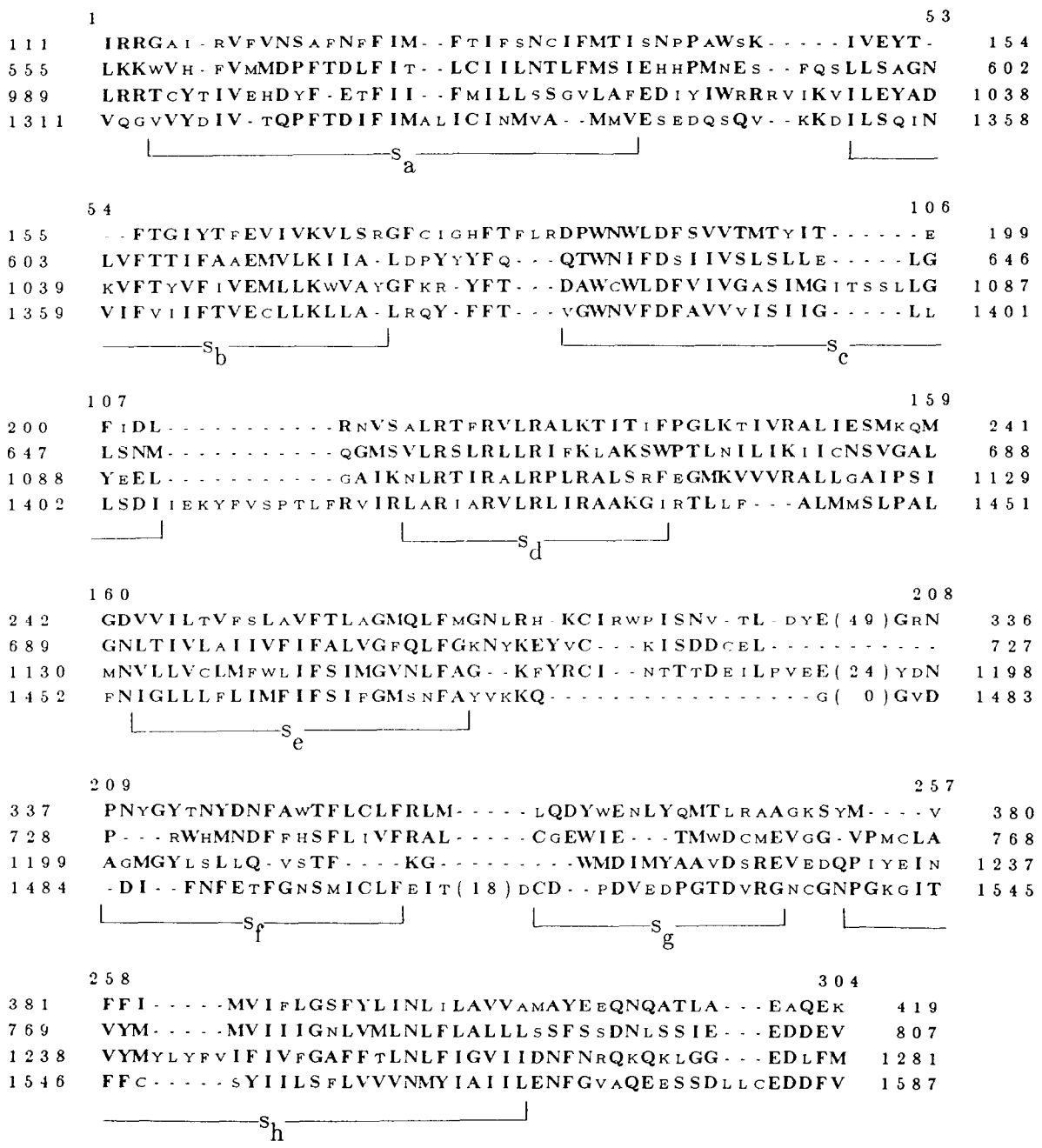

Fig.1. Alignment of the 4 homologous regions of the sodium channel. Region I (residues 111–419) is shown on the top rows, region II (residues 555–807) in the second rows, region III (residues 989–1281) in the third rows and region IV (residues 1311–1587) in the fourth rows. To the left and right of each row are the starting and ending residue numbers for that row. Above and to the left and right of each 4-row alignment are the starting and ending alignment positions, used as the abscissae in fig.3. Similar residues at each alignment position (either identical or within the group [STPAG], [MILV], [HRK], [NDEQ], [FYW]) are indicated in bold-face type. Gaps are indicated as –, and additional non-homologous residues omitted from the alignment are shown as (x), where x = the number of non-homologous residues. Segments S_a–S_h are shown. This alignment is identical to that of Noda et al. [12], except for the region between S_e and S_h.

VMS operating system) using a DEC VAX 11/750 computer (Digital Equipment, Marlboro, MA). The primary sequence [12] was obtained in digital form from the NEWAT database [19]. Hydrophobicity plots were determined as described in [20] using the consensus hydrophobicity data [21]. The hydrophobic power spectral density was obtained by published methods [14,22], using a window of 25 residues, and normalizing with respect to the mean spectral density. The structure prediction algorithm of [23] was used. Homologous sequences were aligned as in [24] using the 'structure-genetic' matrix with a length-independent gap penalty of 5.0 [25] as the basic for a metric. Helical nets were drawn after [26]. Molecular modelling was conducted at the University of California San Diego Chemistry Department Computer Facility, using the 'mms' program developed there.

2.2. *Notation*

Each of the 4 homologous *regions* is referred to by roman numerals I–IV (I closest to the N-terminus). Within each homology region, identified *segments* are referred to by affixing a lowercase subscript (e.g. II_b). Similar segments from all 4 homology regions are referred to as 's_x' where x = [abcdefgh]. In general, when we refer to a segment that also was identified by Noda et al. [12], their notation is enclosed in parentheses for ease of reference, e.g. 's_b (s_2)'. This alternative notation was necessary because we consider the possibility of additional segments between s_5 and s_6.

When referring to specific amino acid sequences, standard one-letter codes are generally used. The symbol '*' is used to refer to any residue. Residue names in brackets (e.g. [ST]) mean that any of the enclosed residues may apply. For example, the sequence '[KR][KR]*[ST]' indicates that residues 1 and 2 may be either arginine or lysine, residue 3 may be any amino acid, and residue 4 may be serine or threonine.

3. RESULTS

3.1. *Overall features*

A graphical summary of many of our results is shown in figs 1 and 2. Inspection of the sequence alignments (fig.1), hydrophobicity plots (fig.2A), and filtered homology matrix plots (not shown), indicate the existence of 4 homologous regions. Within each homology region, there are 5 hydropathic stretches, each 20–35 residues long, called s_1, s_2, s_3, s_5, and s_6 by Noda et al. [12], and s_a, s_b, s_c, s_e, and s_h in this paper. In addition, each homology region contains the sequence $s_d(s_4)$, where positively charged arginine residues repeat with a period of 3. s_a, s_b, and s_c all contain a number of embedded, polar residues. There are additional, weakly hydrophobic sequences found between s_e and s_h in all 4 homology regions (s_f and s_g) which contain a number of acidic or amidic residues.

3.2. *Structure predictions*

There are numerous regions of predicted secondary structure (fig.2). Generally, hydrophobic regions s_a, s_b and s_c display moderate to high predictions of α-helical structure, while s_f and s_h tend toward higher values for β-sheet. Predicted regions of reverse turn are found at several apparent boundaries between structural segments (e.g. bouding I_d, II_d, and preceding I_a, II_a, III_a and IV_a). Several hydrophilic regions are strongly predicted as α-helical, including a stretch preceding I_h, as well as between I/II, II/III, III/IV and following IV.

3.3. *Hydropathic periodicity*

Hydropathic power spectral density plots are illustrated in fig.3. The most salient features of these analyses are the very strong peaks of period 3 (fig.3A and C) approximately centered at residues 215, 660, 1100 and 1430 (fig.3E). These peaks correspond to the 3-fold repeat of the basic residues in $s_d(s_4)$. A 3-fold repeat is intrinsic to a 3_{10} helix. Such a structure appears energetically unfavorable since the strain on the peptide backbone of the helix is combined with a maximal electrostatic repulsion of the positively charged asparagine and lysine residues aligned in parallel along one side of the helix. Alternatively, an α-helical structure for this region would imply that the basic residues form a left handed super-helix with a period of 21 residues (fig.4Ba).

Significant densities are also observed of period 3.5 and period 2. The major density of period 3.5 is associated with $s_b(s_2)$ and $s_c(s_3)$ (fig.3D). It is well visualized in the consensus power spectral density plot of fig.3A and D. Finer-Moore and Stroud [14] identified a similar period 3.5 density in subunits

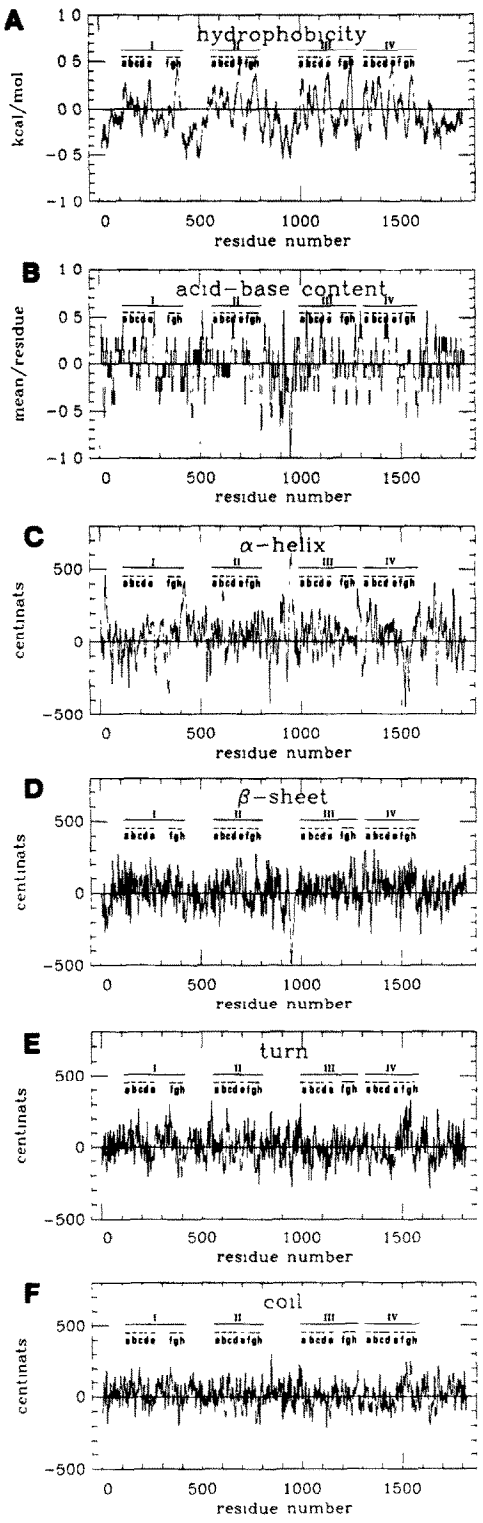

Fig.2. A comparison of the major analytical observations, plotted vs residue number. The positions of each homology region and identified structure segment are indicated. (A) The mean hydrophobicity per residue is shown for a window of 19 residues. (B) The mean 'acid/base' composition for a window of 7 residues is shown. Residues [HRK] are assigned a value of $C = +1$ and residues [DE] a value of $C = -1$. All other residues are assigned a value of $C = 0$, and a moving average $|\ 1/7 \sum_{J=-3}^{J=3} C_J\ |$ is calculated. The calculated structure predictors for α-helix (C), β-sheet (D), turn (E) and coil (F) are plotted vs residue number, following [23].

of the *T. californica* acetylcholine receptor. They speculate that such an amphipathic structure may be associated with the formation of an ion pore wall. If such a stretch were organized as an α-helix, it would have a hydrophobic dipole moment [27] with its polar residues oriented in a direction opposite that of its nonpolar residues. Because the polar side of s_c contains a net excess of acidic residues, it may be a candidate for such a pore-forming structure in a cation-selective channel protein.

The only significant peaks of period 2 are associated with the hydrophobic segment $s_h(s_6)$. This is seen in the consensus power spectral density plot (fig.3A and B), though it appears clearly in the residue sequence only in III_h (centered at residue 1257) (fig.3E). Period 2 behavior might be expected in an amphipathic β-sheet structure. There

Fig.3. Hydropathic power spectral density plots. (A) Consensus power spectrum. Each point represents the mean of the power spectral densities of the residues assigned to be homologous (fig.1). Increasing power is shown as increasing dot density plotted vs period (ordinate) and alignment position (abscissa). Cutoff values were chosen to illustrate salient features. Since the standard deviation normalized with respect to the mean intensity (J/I_m) as in [22] was generally close to 1, values of 10 or greater would be expected to occur by chance with $p<0.001$. Consensus power spectral density for period 2 (B), period 3 (C) and period 3.5 (D). These are the same data illustrated in panel A, displayed to emphasize the power density at structurally significant periods. (E) Power spectral density vs residue for the entire protein, with increasing power shown as increasing dot density (see inset). The location of transmembrane segments a–h is indicated.

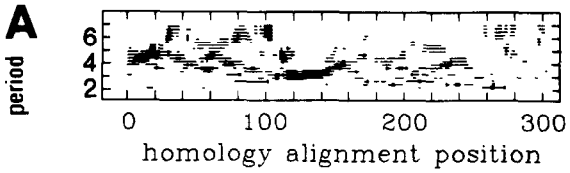
A
period
6
4
2
0
100
200
300
homology alignment position

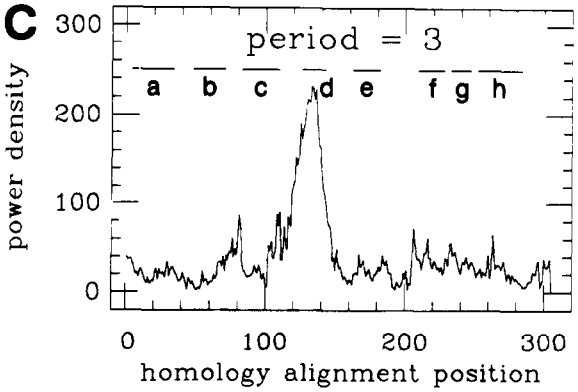
C
period = 3
a b c d e f g h
power density
300
200
100
0
0
100
200
300
homology alignment position

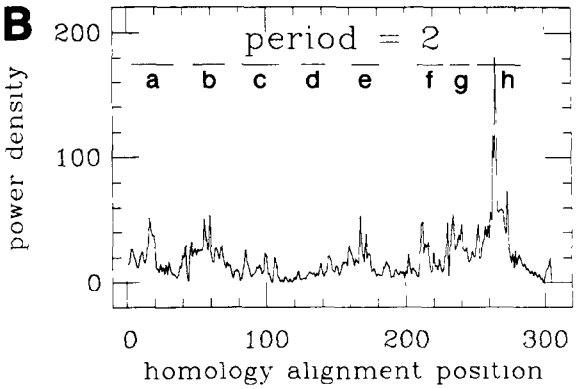
B
period = 2
a b c d e f g h
power density
200
100
0
0
100
200
300
homology alignment position

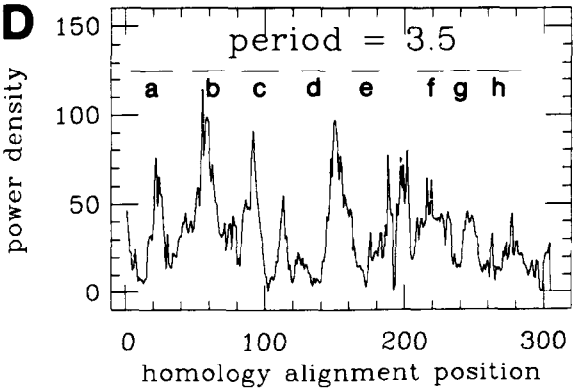
D
period = 3.5
a b c d e f g h
power density
150
100
50
0
0
100
200
300
homology alignment position

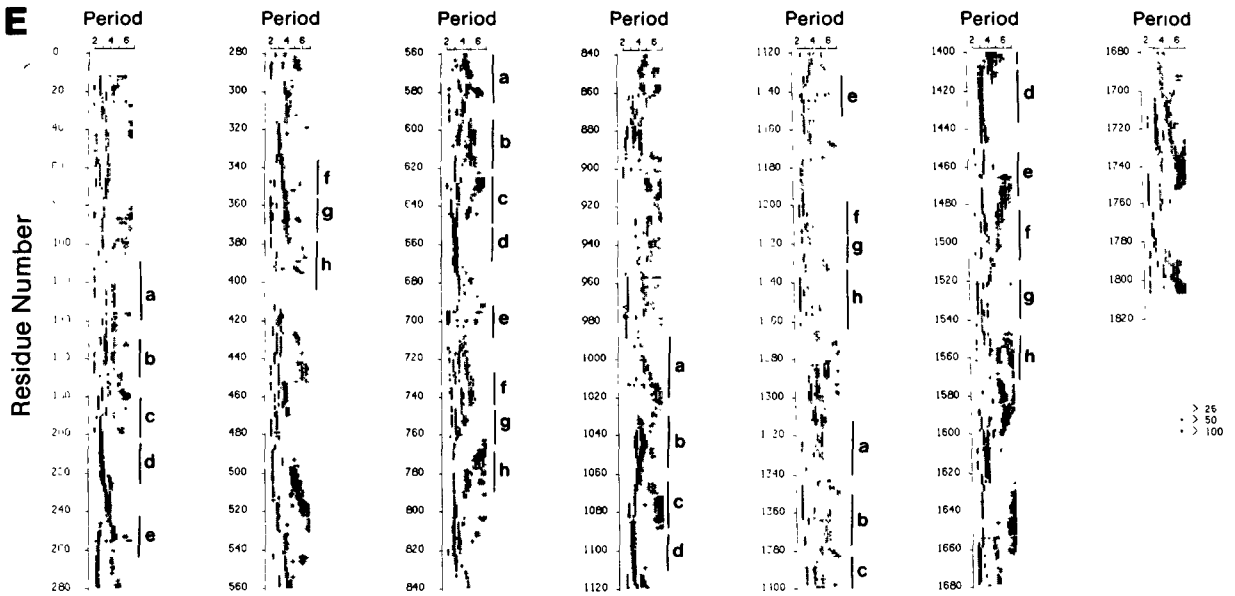
E
Period
Residue Number
a
b
c
d
e
f
g
h
> 25
> 50
> 100

is a significant peak at period 3.75–4.0 in the consensus power spectral density plot, centered on s_g. This arises from an alternation of acidic (D or E) or amidic (N or Q) residues with non-polar residues (fig.4Bb).

The 4 amphipathic segments postulated to be involved in channel lining are represented as helical nets in fig.4A. The polar residues X are indicated as *X*. Each segment has 21 residues. Since the spacing between residues is 1.5 Å in an α-helix, each segment s_c would be ~32 Å long. This length is sufficient to traverse the hydrocarbon core of the lipid bilayer [28]. Fig.4B is a helical net representation of segments II_d (654–672) and II_g (747–764). Similar segments from all homologous regions may contribute to the voltage sensor of the sodium channel protein. Such structures appear to be well-suited to interact electrostatically, thereby forming a cluster of high electrical dipole moment, with little net charge. The postulated cluster would facilitate the incorporation of hydrophilic residues within the otherwise hydrophobic membrane domains of the protein. A possible role for such dipolar cluster in the voltage-dependent gating kinetics of the sodium channel is considered below.

Interacting α-helic pairs are observed to cluster at relative orientations of approx. 20° [13,26], corresponding to an interaction between residues spaced 3 apart on one helix and 4 apart on the other. Examples of possible period −3/period −4 interactions between s_d and s_g are illustrated as helical nets in fig.4Bc.

3.4. *Specific sequences*

The α-subunit of the the rat brain sodium channel is a good substrate of cAMP-dependent protein kinase [29,30]. From the known specificity of this enzyme ([KR][KR]*[ST] or [KR][KR]**[ST]) [31],

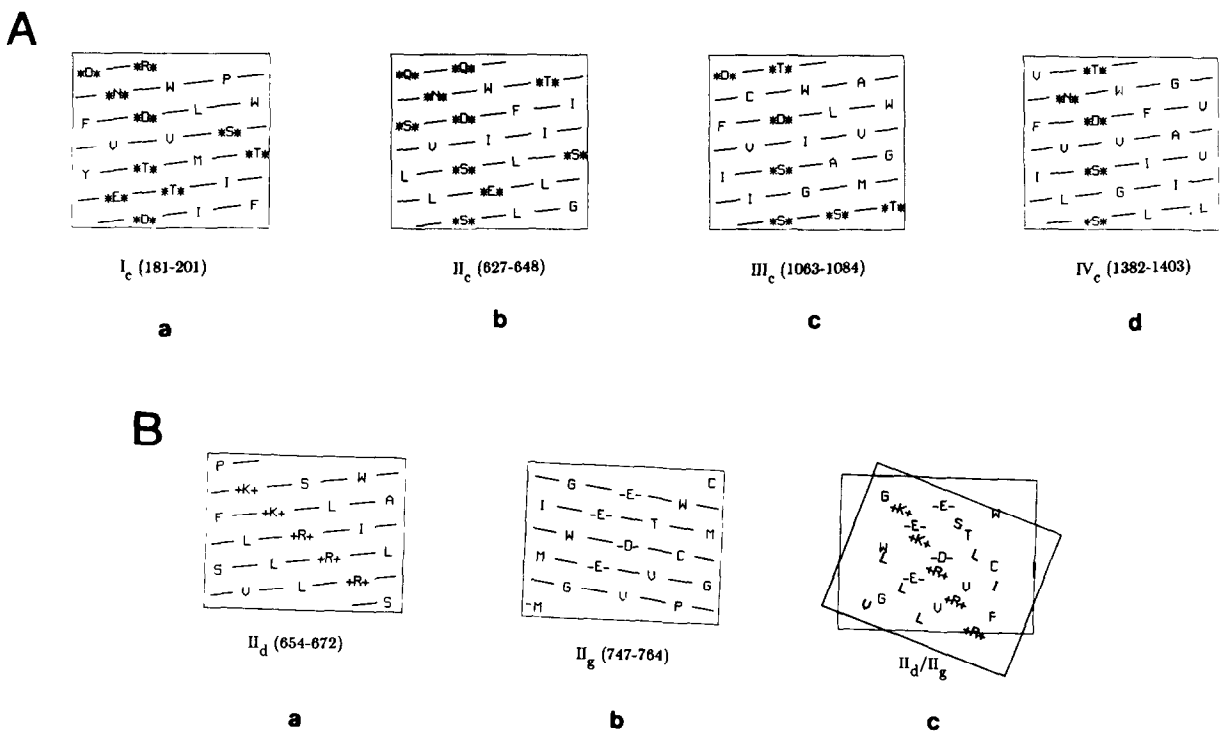

Fig.4. Helical nets of selected portions of the protein. (A) Helical net representation of amphipathic segments I_c–IV_c. Polar residues X = [HRKNDEQ ST] are indicated as *X*. Each segment has 21 residues. Considering that for an α-helix residues are separated by 1.5 Å, each segment would be 32 Å long. (B) Helical net representation at an equivalent radius of 5 Å of (a) II_d (654–672) face down, (b) II_g (747–764) face up, (c) panel Bb superimposed on Ba in an antiparallel orientation at an angle of ~20° to indicate possible interactions between acidic and basic polar groups in a II_d/II_g α-helical pair.

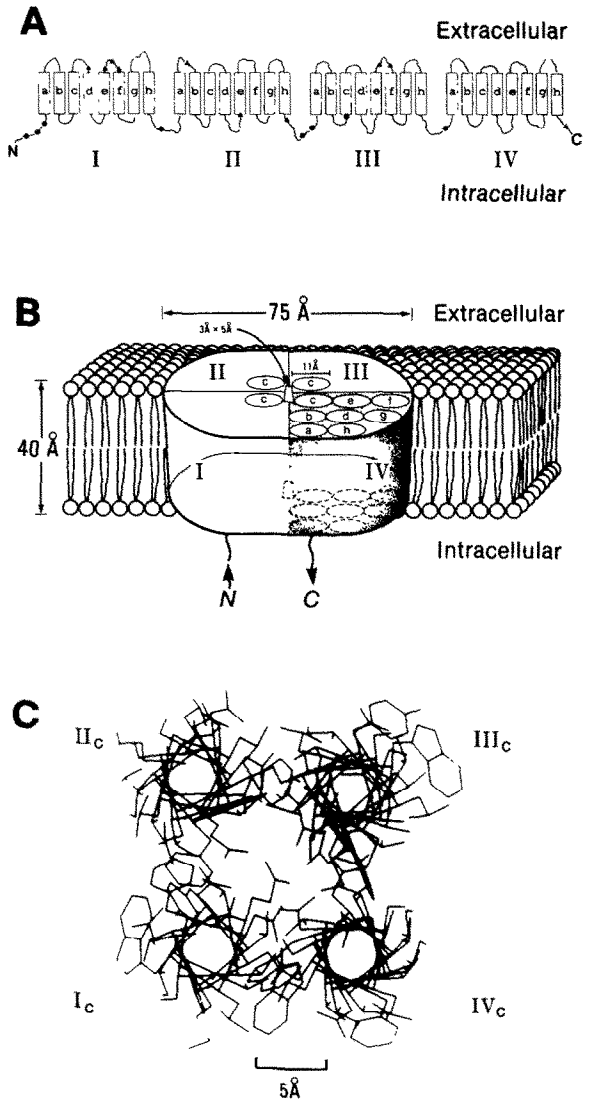

Fig.5. Hypothetical structural model of the sodium channel. (A) One-dimensional representation of the cytoplasmic, transmembrane, and extracellular domains. Four homologous regions, each consisting of 8 membrane-spanning helical segments are shown. Adjacent segments traverse the membrane in antiparallel orientation. (●) Potential phosphorylation sites, (▲) potential glycosylation sites. (B) Schematic tertiary structure model of the channel, showing the 4 homology regions organized in a pseudo-radially symmetric array. Note that the structure is close-packed. Carbohydrate moiety is omitted. (C) Orthographic projection of a possible ion pore formed by amphipathic helices s_c oriented in parallel. Distance scale indicates the spacing between Asp 188 (I_c) and Asp 634 (II_c).

potential phosphorylation sites are identified at residues Ser 7, Thr 17, Thr 35, Ser 444, Ser 846, Thr 862, Thr 1063, and Ser 1297. It is significant that all the putative phosphorylation sites are predicted to be in the cytoplasmic domain of the protein, and all, but Thr 1063, are found near the N-terminus or between homology regions. Noda et al. [12] suggested that potential glycosylation sites occur at asparagine residues 205, 278, 288, 317, 591, 690, 797, 1160, 1174 and 1806. The relative locations of the potential phosphorylation and glycosylation sites with respect to identified structural segments are shown in fig.5A.

4. DISCUSSION

Currently available methods for secondary structure prediction, such as those employed in this study, are at an early stage of development, especially when applied to integral membrane proteins. For the sodium channel, in addition, biophysical data other than electrophysiological measurements (e.g. CD, ORD, IR or NMR) are sparse or non-existent. Therefore, any model is likely to be incomplete, ambiguous and partly erroneous. However, in the absence of the exact X-ray structure, the use of models such as that described here is justified as a guide to the design and interpretation of experiment.

In considering possible structural models of the sodium channel protein that might account for aspects of ion flow through the channel as well as voltage-dependent channel opening and closing (gating), and which are consistent with the primary structure, the main assumptions were: (i) membrane-spanning regions have an organized secondary structure, probably α-helical (cf. [27]); (ii) the absence of a hydrophobic leader sequence suggests that both C- and N-termini are cytoplasmic, [12]; (iii) the pseudo symmetry generated by 4 homologous regions (along with (ii) above), implies an even number of transmembrane segments per homologous region [12]; (iv) the voltage-dependent change in dipole moment (observed as gating current) implies displacement of charges buried within the intramembranous, hydrophobic interior of the protein (cf. [32]); (v) at physiological pH, glutamate and aspartate residues are negatively charged and lysine, arginine and asparagine groups are positively charged. The

Table 1

Key features of four models of the sodium channel protein

Features	Noda and collaborators [12]	Guy and Seetharamulu [17]
Method	Kyte and Doolittle Homologies Secondary structure predictors	Calculations of water, protein and lipid exposure of portions of putative α-helices and β-strands. Visual inspection and computer graphics Model Building
Homologous domains: repeat number	4	4
C- and N-termini	Intracellular	Intracellular
Transmembrane passages per homologous domain	Even	Even
Transmembrane passages/domain	4–[6]	8
Channel lining:	S_1 S_3 [S_2] α-helix, amphipathic Not S_4 Neutral	'S_1 and S_2 unlikely' 3 short (−) amphipathic α-helices + 1 (−) amphipathic β-strand (S_7) interacting with 4 (+) α-helix (S_4). Neutral
Selectivity 'filter'	Channel lining Neutral or S_1 and S_3: (−)	Channel lining Neutral No hypothesis about filter
Voltage sensor: Activation	4(S_4)→4 gating charges [probably cytoplasmic]	S_4 - intramembranous $\vec{E}$-field induced screw-like motion of S_4
Inactivation	Clusters of glutamates between (800–960) [probably cytoplasmic]	No hypothesis
cAMP-dependent phosphorylation sites (total = 8)	8/8	Cytoplasmic (8/8)
N-Glycosylation sites (total = 10)	Extracellular 6/10	Extracellular (7/10–10/10)

location of these charged groups within the protein/membrane interior would be energetically favored via the formation of ion pairs (cf.[33,34]); (vi) ion diffusion through the channel proceeds via a water-filled pore, whose walls consist of amphipathic structures, including one or more acidic groups within the pore.

Fig.5B illustrates a schematic representation of one hypothetical tertiary structure consistent with these assumptions and our observations. This structure is pseudo-radially symmetric. At its center, helical regions I_c, II_c, III_c and IV_c come together with their hydrophilic surfaces inwards to form a putative ion channel. We note that approx-

Greenblatt and collaborators	Kosower [18]
Kyte and Doolittle Power spectral density Secondary structure predictors Homologies Computer graphics	Chemical logic Single group rotation
4	No homologous domains assigned
Intracellular	Intracellular
Even 8	20 bilayer helices: 14 hydrophobic, 6 amphipathic
s_c amphipathic helix	4 positively charged 3_{10} helices (210–227; 657–674; 1092–1109; 1417–1434)
Neutral to (−)	2 negatively charged 3_{10} helices (893–910; 942–959)
Channel lining s_c (−) Negative pore	911–941 Charge gradient from extracellular to intracellular (−3,0,0,0,0,+1)
s_d – intramembranous $\bar{E}$-field induced displacements of dipolar clusters between 4 (s_d) and 4 (s_g,s_f)	911–941 793–892
$\bar{E}$-field induced rearrangement of ion pairs in the dipolar cluster s_d, s_g, s_c	Electric field induced displacement of charges
Cytoplasmic 8/8	8/8 cytoplasmic
Extracellular (7/10–10/10)	Extracellular (7/10)

imating the helices by 4 cylinders of diameter 10.5 Å [28] would create a central pore 4.2 Å across at its narrowest extent (the effective dimension of the sodium channel at its narrowest point is 3 Å by 5 Å) [35]. A computer-generated molecular model of the pore-forming structure is illustrated in fig.5C.

In each region, s_d is indicated at the center of a clustered structure of high dipole moment (fig.5B). Similar buried ion pairs have been observed crystallographically (e.g. Arg CD3 and Asp E3 of myoglobin [36]). s_a, s_b, s_e, s_h and s_f in each region are illustrated to occur at the interfaces between homologous regions, providing favorable and extensive hydrophobic boundaries.

How might such a structure explain the electrophysiological phenomenology? The key feature is the sensitivity to applied electric fields of the 4 dipolar clusters each formed by s_d, s_g and s_c. Voltage-controlled gating arises from the electric field-induced disruption of multiple ion pairs buried within the hydrophobic, intramembranous protein interior. This consideration suggests that, when the channel is closed and the membrane is hyperpolarized, the transmembrane voltage pulls apart the ion pairs, stabilizing a relatively large transmembrane electrical dipole moment. As the membrane is depolarized, these pairs are allowed to relax towards one another. A change in dipole moment of 1000 debye [35] would require that 30 ion pairs each shift by approx. 8 Å in a direction normal to the membrane surface. This may be compared to a movement between hemoglobin subunits of 6.5 Å upon binding of oxygen, as observed crystallographically [13]. This transmembrane relaxation may change the lateral interaction between s_d and the ion pore structure (s_c), allowing cations to diffuse through the pore. Such a new state (activation) may be unstable and decay to another state associated with channel closure (inactivation).

The major features of the sodium channel protein models are compared in table 1. All models presume the N- and C-termini, as well as the region between II and III to be cytoplasmic. Thus, a key experimental test of all models would be to determine the sidedness of these regions, perhaps via monoclonal antibodies [37] or proteolysis [38]. The model of Noda et al. [12] predicts that $s_c(s_3)$ and $s_d(s_4)$ are cytoplasmic, while the other models propose them to be interior to the membrane, a distinction that may be testable through antibody studies. The identification of phosphorylation sites should prove useful in the identification of cytoplasmic domains. The differences between our model and that of Guy and Seethramulu appear more difficult to probe experimentally because segments predicted to be transmembrane are

similar. Nearest neighbor analysis of adjacent helices by means of cleavable crosslinkers and structure determination of crosslinked products could give clues about the distinct helical clusters predicted by the two models. Further computational studies may provide additional information on the thermodynamic feasibility of such models.

ACKNOWLEDGEMENTS

We are indebted to R. Guy for sharing with us his model before publication, R. Doolittle and M. Johnson for allowing us access to their sequence bank, R. Stroud and B. Keller for valuable discussions, the University of California San Diego Chemistry Department for use of the computer graphics facility and Laura Castrejon for valuable assistance. This work was supported by grants from the National Institutes of Health (EY-02084) and the Department of the Army Medical Research (17-82-C2221).

REFERENCES

[1] Hodgkin, A.L. and Huxley, A.F. (1952) J. Physiol. 117, 500–544.
[2] Agnew, W.S., Levinson, S.R., Brabson, J.S. and Raftery, M.A. (1978) Proc. Natl. Acad. Sci. USA 75, 2606–2610.
[3] Barchi, R.L. (1983) J. Neurochem. 40, 1377–1385.
[4] Lombet, A. and Lazdunski, M. (1984) Eur. J. Biochem. 141, 651–666.
[5] Hartshorne, R.P. and Catterall, W.A. (1984) J. Biol. Chem. 259, 1667–1675.
[6] Rosenberg, R.L., Tomiko, S.A. and Agnew, W.S. (1984) Proc. Natl. Acad. Sci. USA 81, 1239–1243.
[7] Talvenheimo, J.A., Tamkun, M.M. and Catterall, W.A. (1982) J. Biol. Chem. 257, 11868–11871.
[8] Weigele, J.B. and Barchi, R.L. (1982) Proc. Natl. Acad. Sci. USA 79, 3651–3655.
[9] Rosenberg, R.L., Tomiko, S.A. and Agnew, W.S. (1984) Proc. Natl. Acad. Sci. USA 81, 5594–5598.
[10] Hartshorne, R.P., Keller, B., Talvenheimo, J., Catterall, W.A. and Montal, M. (1985) Proc. Natl. Acad. Sci. USA 82, 240–244.
[11] Hanke, W., Boheim, G., Barhanin, J., Pauron, D. and Lazdunski, M. (1984) EMBO J. 3, 509–515.
[12] Noda, M., Shimizu, S., Tanabe, T., Takai, T., Kayano, T., Ikeda, T., Takahashi, H., Nakayama, H., Kanaoka, Y., Minamino, N., Kangawa, K., Matsuo, H., Rafterty, M.A., Hirose, T., Notake, M., Inayama, S., Hayashida, H., Miyata, T. and Numa, S. (1984) Nature 312, 121–127.
[13] Creighton, T.E. (1984) Proteins, W.H. Freeman, New York.
[14] Finer-Moore, J. and Stroud, R.M. (1984) Proc. Natl. Acad. Sci. USA 81, 155–159.
[15] Guy, H.R. (1984) Biophys. J. 45, 249–261.
[16] Mishina, M., Tobimatsu, T., Imoto, K., Tanaka, K., Fujita, Y., Fukuda, K., Kurasaki, M., Takahashi, H., Morimoto, Y., Hirose, T., Inayama, S., Takahashi, T., Kuno, M. and Numa, S. (1985) Nature 313, 364–369.
[17] Guy, H.R. and Seetharamulu, P. (1985) Proc. Natl. Acad. Sci. USA, in press.
[18] Kosower, E.M. (1985) FEBS Lett. 182, 234–242.
[19] Doolittle, R. (1981) Science 214, 149–159.
[20] Kyte, J. and Doolittle, R. (1982) J. Mol. Biol. 157, 105–132.
[21] Eisenberg, D., Weiss, R.M., Terwilliger, T.C. and Wilcox, W. (1982) Faraday Symp. Chem. Soc. 17, 109–120.
[22] McLachlan, A.D. and Stewart, M. (1976) J. Mol. Biol. 103, 271–298.
[23] Garnier, J., Osguthorpe, D.J. and Robson, B. (1978) J. Mol. Biol. 120, 97–120.
[24] Needleman, S.B. and Wunsch, C.D. (1970) J. Mol. Biol. 48, 443–453.
[25] Feng, D.F., Johnson, M.S. and Doolittle, R.F. (1985) J. Mol. Evol. 21, 112–125.
[26] Chothia, C. (1984) Annu. Rev. Biochem. 53, 537–572.
[27] Eisenberg, D. (1984) Annu. Rev. Biochem. 53, 595–623.
[28] Blaurock, A.E. and Wilkins, M.H.F. (1969) Nature 223, 906–909.
[29] Costa, M.R.C., Casnelli, J.E. and Catterall, W.A. (1982) J. Biol. Chem. 257, 7918–7921.
[30] Costa, M.R.C. and Catterall, W.A. (1984) J. Biol. Chem. 259, 8210–8218.
[31] Kemp, B.E., Graves, D.J., Benjamini, E. and Krebs, E.G. (1977) J. Biol. Chem. 252, 4888–4894.
[32] Armstrong, C.M. (1981) Physiol. Rev. 61, 644–683.
[33] Gemant, A. (1962) Ions in Hydrocarbons, Wiley, New York.
[34] Warshel, A. and Russell, S.T. (1984) Q. Rev. Biophys. 17, 283–422.
[35] Hille, B. (1984) Ionic Channels of Excitable Membranes, Sinauer, Sunderland, MA.
[36] Kendrew, J.C., Watson, H.C., Strandberg, B.E., Dickerson, R.E., Phillips, D.C. and Shore, V.C. (1961) Nature 190, 666–670.
[37] Criado, M., Hochschwender, S., Sarin, V., Fox, J.L. and Lindstrom, J. (1985) Proc. Natl. Acad. Sci. USA 82, 2004–2008.
[38] Conti-Tronconi, B.M., Hunkapiller, B.M. and Raftery, M.A. (1984) Proc. Natl. Acad. Sci. USA 81, 2631–2634.